Plasmonic silicon solar cells: impact of material quality and geometry

Celine Pahud,[1,*] Olindo Isabella,[2] Ali Naqavi,[3] Franz-Josef Haug,[1] Miro Zeman,[2] Hans Peter Herzig,[3] and Christophe Ballif[1]

[1]*Ecole Polytechnique Fédérale de Lausanne (EPFL), Institute of Microengineering (IMT), Photovoltaics and thin film electronics laboratory, CH-2000 Neuchatel, Switzerland*
[2]*Delft University of Technology, Photovoltaic Materials and Devices group, Mekelweg 4, 2628 CD, Delft, the Netherlands*
[3]*Ecole Polytechnique Fédérale de Lausanne (EPFL), Institute of Microengineering (IMT), Optics, CH-2000 Neuchatel, Switzerland*

[*]*celine.pahud@epfl.ch*

Abstract: We study n-i-p amorphous silicon solar cells with light-scattering nanoparticles in the back reflector. In one configuration, the particles are fully embedded in the zinc oxide buffer layer; In a second configuration, the particles are placed between the buffer layer and the flat back electrode. We use stencil lithography to produce the same periodic arrangement of the particles and we use the same solar cell structure on top, thus establishing a fair comparison between a novel plasmonic concept and its more traditional counterpart. Both approaches show strong resonances around 700 nm in the external quantum efficiency the position and intensity of which vary strongly with the nanoparticle shape. Moreover, disagreement between simulations and our experimental results suggests that the dielectric data of bulk silver do not correctly represent the reality. A better fit is obtained by introducing a porous interfacial layer between the silver and zinc oxide. Without the interfacial layer, e.g. by improved processing of the nanoparticles, our simulations show that the nanoparticles concept could outperform traditional back reflectors.

OCIS codes: (310.6845) Thin film devices and applications; (250.5403) Plasmonics.

References and links

1. H. Deckman, C. Wronski, H. Witzke, and E. Yablonovitch, "Optically enhanced amorphous silicon solar cells," Appl. Phys. Lett. **42**(11), 968–970 (1983).
2. A. Banerjee and S. Guha, "Study of back reflectors for amorphous silicon alloy solar cell application," J. Appl. Phys. **69**(2), 1030–1035 (1991).
3. O. Kluth, B. Rech, L. Houben, S. Wieder, G. Schöpe, C. Beneking, H. Wagner, A. Löffl, and H. Schock, "Texture etched ZnO: Al coated glass substrates for silicon based thin film solar cells," Thin Solid Films **351**(1), 247–253 (1999).
4. S. Fay, J. Steinhauser, S. Nicolay, and C. Ballif, "Polycrystalline ZnO: B grown by LPCVD as TCO for thin film silicon solar cells," Thin Solid Films **518**(11), 2961–2966 (2010).
5. S. Guha and J. Yang, "Progress in amorphous and nanocrystalline silicon solar cells," J. Non-Cryst. Solids **352**(9-20), 1917–1921 (2006).
6. S. Benagli, D. Borello, E. Vallat-Sauvain, J. Meier, U. Kroll, J. Hoetzel, J. Bailat, J. Steinhauser, M. Marmelo, G. Monteduro, and L. Castens, "High efficiency amorphous silicon devices on LP-CVD-ZnO TCO prepared in industrial KAI R&D reactor," Conference Record 23th EU-PVSEC 3BO.9.3 (2009).
7. J. Yang, A. Banerjee, and S. Guha, "Triple-junction amorphous silicon alloy solar cell with 14.6% initial and 13.0% stable conversion efficiencies," Appl. Phys. Lett. **70**(22), 2975–2977 (1997).

#190715 - $15.00 USD Received 17 May 2013; revised 4 Jul 2013; accepted 4 Jul 2013; published 16 Jul 2013

8. H. Lee, S. Ahn, S. Lee, and J. Choi, "Silicon thin film technology applications for low cost and high efficiency photovoltaics," 21st International Photovoltaic Science and Engineering Conference, Fukuoka 4A–2I–01 (2011).
9. K. Catchpole and S. Pillai, "Absorption enhancement due to scattering by dipoles into silicon waveguides," J. Appl. Phys. **100**, 044504 (2006).
10. H. Atwater and A. Polman, "Plasmonics for improved photovoltaic devices," Nature Mater. **9**(3), 205–213, (2010).
11. R. Santbergen, T. Temple, R. Liang, A. Smets, R. Swaaij, and M. Zeman, "Application of plasmonic silver island films in thin-film silicon solar cells," J. Opt. **14**, 024010 (2012).
12. C. Rockstuhl and F. Lederer, "Photon management by metallic nanodiscs in thin film solar cells," Appl. Phys Lett. **94**, 213102 (2009).
13. V. Ferry, A. Polman, and H. Atwater, "Modeling light-trapping in nanostructured solar cells," ACS Nano **5**(12), 10055–10064 (2011).
14. R. Biswas, and D. Zhou, "Simulation and modelling of photonic and plasmonic crystal back reflectors for efficient light trapping," Phys. Status Solidi A. **207**(3), 667–670 (2010).
15. U. Paetzold, E. Moulin, B. Pieters, U. Rau, and R. Carius, "Optical simulations of microcrystalline silicon solar cells applying plasmonic reflection grating back contacts," J. Photon. Energy **2**(1), 027002 (2012).
16. F. Tsai, J. Wang, J. Huang, Y. Kiang, and C. Yang, "Absorption enhancement of an amorphous Si solar cell through surface plasmon-induced scattering with metal nanoparticles," Opt. Express **18**(102), A207–A220 (2010).
17. J. Wang, F. Tsai, J. Huang, C. Chen, N. Li, Y. Kiang, and C. Yang, "Enhancing InGaN-based solar cell efficiency through localized surface plasmon interaction by embedding Ag nanoparticles in the absorbing layer," Opt. express, **18**(3), 2682–2694 (2010).
18. H.R. Stuart, D.G. Hall, "Absorption enhancement in silicononinsulator waveguides using metal island films," Appl. Phys. Lett. **69**, 2337 (1996).
19. F. Beck, A. Polman, and K. Catchpole, "Tunable light trapping for solar cells using localized surface plasmons," J. Appl. Phys. **105**, 114310 (2009).
20. O. El Daifa, L. Tong, B. Figeys, K. Van Nieuwenhuysen, A. Dmitriev, P. Van Dorpe, I. Gordon and F. Dross, "Front side plasmonic effect on thin silicon epitaxial solar cells," Sol. Energy Mater. Sol. Cells **104**, 58-63 (2012).
21. R. Santbergen, R. Liang, and M. Zeman, "Amorphous silicon solar cells with silver nanoparticles embedded inside the absorber layer," Materials Research Society Symposium Proceedings 1245. Cambridge Univ Press (2010).
22. E. Moulin, J. Sukmanowski, P. Luo, R. Carius, F. Royer, and H. Stiebig, "Improved light absorption in thin-film silicon solar cells by integration of silver nanoparticles," J. Non-Cryst. Solids **354**(19), 2488–2491 (2008).
23. C. Eminian, F. Haug, O. Cubero, X. Niquille, and C. Ballif, "Photocurrent enhancement in thin film amorphous silicon solar cells with silver nanoparticles," Prog. Photovolt: Res. Appl. **19**(3), 260–265 (2011).
24. H. Mizuno, H. Sai, K. Matsubara, and M. Kondo, "Light trapping by Ag nanoparticles chemically assembled inside thin-film hydrogenated microcrystalline Si solar cells," Jpn. J. Appl. Phys. **51**, 042302 (2012).
25. H. Tan, R. Santbergen, A. Smets, and M. Zeman, "Plasmonic light trapping in thin-film silicon solar cells with improved self-assembled silver nanoparticles," Nano Lett. **12**(8), 4070–4076 (2012).
26. C. Pahud, V. Savu, M. Klein, O. Vazquez-Mena, J. Brugger, and C. Ballif, "Stencil-nanopatterned back reflectors for thin-film amorphous silicon n-i-p solar cells," IEEE J. Photovolt. **3**(1), 22–26, (2013).
27. O. Vazquez-Mena, T. Sannomiya, L. Villanueva, J. Voros, and J. Brugger, "Metallic nanodot arrays by stencil lithography for plasmonic biosensing applications," ACS Nano **5**(2), 844–853 (2011).
28. M. Klein, F. Montagne, N. Blondiaux, O. Vazquez-Mena, H. Heinzelmann, R. Pugin, J. Brugger, and V. Savu, "SiN membranes with submicrometer hole arrays patterned by wafer-scale nanosphere lithography," J. Vac. Sci. Technol. B **29**(2), 012–021 (2011).
29. http://www.ansys.com.
30. O. Isabella, S. Solntsev, D. Caratelli, and M. Zeman, "3-D optical modeling of thin-film silicon solar cells on diffraction gratings," Prog. Photovolt: Res. Appl. **21**(1), 94–108 (2013).
31. C. Eisele, C. Nebel, and M. Stutzmann, "Periodic light coupler gratings in amorphous thin film solar cells," J. Appl. Phys. **89**, 7722 (2001).
32. C. Haase and H. Stiebig, "Thin-film silicon solar cells with efficient periodic light trapping texture," Appl. Phys. Lett. **91**, 061116 (2007).
33. O. Isabella, A. Campa, M. Heijna, W. Soppa, R. van Ervan, R. Franken, H. Borg, and M. Zeman, "Diffraction gratings for light trapping in thin-film silicon solar cells," Conference Record of the 23rd European Photovoltaic Solar Energy Conference 2320–2324 (2008).
34. A. Naqavi, K. Söderström, F. Haug, V. Paeder, T. Scharf, H. Herzig, and C. Ballif, "Understanding of photocurrent enhancement in real thin film solar cells: towards optimal one-dimensional gratings," Opt. Express **19**(1), 128–140 (2011).
35. Z. Yu, A. Raman, and S. Fan, "Thermodynamic upper bound on broadband light coupling with photonic structures," Phys. Rev. Lett. **109**(17), 173901 (2012).
36. A. Naqavi, F. Haug, C. Ballif, T. Scharf, and H. Herzig, "Limit of light coupling strength in solar cells," Appl.

#190715 - $15.00 USD Received 17 May 2013; revised 4 Jul 2013; accepted 4 Jul 2013; published 16 Jul 2013

Phys. Lett. **102**(13), 1113 (2013).
37. P. Johnson and R. Christy, "Optical constants of the noble metals," Phys. Rev. B **6**(12), 4370 (1972).
38. E. Palik, *Handbook of Optical Constants of Solids* (Academic press **3** 1998),
39. L. Ingersoll, "The dispersion of metals in the infra-red spectrum," Astrophys. J. **32**(265), (1910).
40. M. Green and S. Pillai, "Harnessing plasmonics for solar cells," Nature Photon. **6**(3), 130–132 (2012).
41. D. Nash and J. Sambles, "Surface plasmon-polariton study of the optical dielectric function of silver," J. Mod. Opt. **43**(1), 81–91 (1996).
42. F. Parmigiani, E. Kay, T. Huang, J. Perrin, M. Jurich, and J. Swalen, "Optical and electrical properties of thin silver films grown under ion bombardment," Phys. Rev. B **33**(2), 879 (1986).
43. D. Sainju, P. van den Oever, N. Podraza, M. Syed, J. Stoke, J. Chen, X. Yang, X. Deng, and R. Collins, "Origin of optical losses in Ag/ZnO back-reflectors for thin film Si photovoltaics," in Photovoltaic Energy Conversion, Conference Record of the 2006 IEEE 4th World Conference on **2**, 1732–1735 (2006).
44. K. Kelly, E. Coronado, L. Zhao, and G. Schatz, "The optical properties of metal nanoparticles: the influence of size, shape, and dielectric environment," J. Phys. Chem. B **107**(3), 668–677 (2003).
45. K. Söderström, F. Haug, J. Escarré, C. Pahud, R. Biron, and C. Ballif, "Highly reflective nanotextured sputtered silver back reflector for flexible high-efficiency n–i–p thin-film silicon solar cells," Sol. Energy Mater. Sol. Cells **95**(12), 3585–3591 (2011).
46. C. Lee, T. Lee, and Y. Jen, "Ion-assisted deposition of silver thin films," Thin Solid Films **359**(1), 95–97 (2000).
47. Z. Holman, M. Filipic, A. Descoeudres, S. De Wolf, F. Smole, M. Topic, and C. Ballif, "Infrared light management in high-efficiency silicon heterojunction and rear-passivated solar cells," J. Appl. Phys. **113**, 013107 (2013).

1. Introduction

Thin-film silicon solar cells strongly rely on light-trapping schemes to achieve high efficiencies. Due to their relatively low absorption in the near-infrared wavelengths, light management is necessary to enhance their photocurrent [1]. The conventional approach consists of growing silicon layers on a randomly textured substrate or transparent conductive oxide (TCO) layer [2–5]. Efficient scattering occurs at the rough TCO/silicon interface because of the refractive index mismatch between the two materials. To date, the most efficient solar cells are based on this approach, both in superstrate (p-i-n) and substrate (n-i-p) configurations [6–8].

Light scattering by metallic nanoparticles is an alternative and promising approach for light trapping. Silver or gold subwavelength particles embedded in a dielectric support localized plasmonic modes that have a large scattering cross section [9, 10]. The scattering efficiency strongly depends on the nanoparticle size, as particles smaller than 30 nm tend more to absorb light than to scatter it [11]. Therefore, the nanoparticles need to be carefully designed to avoid parasitic absorption and to enhance photocurrent generation in the solar cell. Modelling results predict that plasmonic concepts can yield significant photocurrent enhancement in thin-film silicon solar cells [12–17].

Experimental results suggest that plasmonic cells must be designed carefully; the incorporation of nanoparticles on the front contact of solar cells, as originally suggested by Stuart et al. [18], resulted in significant photocurrent loss in the visible range when applied to crystalline solar cells [19, 20], while embedding them in the absorber layer of thin-film cells was found to disturb current collection [21]. Therefore, integration into the back reflector represents the most successful option [22–24]. However, it remains difficult to assess the true benefit of plasmonic concepts from a comparison to flat reference cells since the embedding of nanoparticles in the rear electrode also adds texture to the active layers. Recently, Tan et al. presented a plasmonic back reflector that yields a photocurrent as high as that generated by a conventional random reflector, alas one with very different texture [25].

In this contribution, we compare a nanoparticles back reflector with a conventional grating back reflector for thin-film solar cells. In our previous work [26], a fair and conclusive assessment is achieved by using stencil lithography for the fabrication of identical arrays of disc-shaped nanoparticles and by co-depositing the solar cells and front electrodes. Our experiments show that the nanoparticles back reflector yields a lower photocurrent density than

#190715 - $15.00 USD Received 17 May 2013; revised 4 Jul 2013; accepted 4 Jul 2013; published 16 Jul 2013

its conventional counterpart. Here we interpret our experimental findings with rigorous optical simulations, taking into account intermixing in the interfacial region between silver and zinc oxide (ZnO). Our results suggest that the nanoparticles are more susceptible to parasitic losses in this region. Assuming that shortcomings in the fabrication process can be eliminated, silver nanoparticles of high quality would have the potential to scatter light more efficiently than conventional back reflectors.

2. Methods

2.1. Solar cell fabrication

Our back reflectors consist of a flat silver film of 160 nm thickness which was deposited on glass. For the nanoparticles reflector, the silver film was covered with 35 nm of ZnO. Subsequently, silver nanoparticles were fabricated by evaporation through a hexagonal array of holes in a stencil membrane. In order to guarantee identical geometry, we employed stencil lithography [27, 28]. The nanoparticles and the grating back reflectors were completed by depositing ZnO films of 35 and 70 nm, respectively. Figure 1 illustrates that the former consists of nanoparticles embedded in ZnO, while in the latter, the nanoparticles are in contact with the flat silver film. The period of the hexagonal array is 430 nm, and the diameter and height of the nanoparticles are 220 nm and 40 nm, respectively. Further details on the back reflector fabrication are reported in our previous work [26]. As seen in Fig. 1, the intrinsic layer and the front electrode have the same geometry in both configurations, slight inhomogeneities notwithstanding. Therefore a fair comparison of the back reflectors' light-trapping performances is possible.

Amorphous silicon (a-Si:H) solar cells with a $\sim$220-nm-thick intrinsic layer were deposited in the substrate configuration onto the back reflectors. The front electrode is composed of a 70-nm-thick indium tin oxide (ITO) layer that acts as an anti-reflection coating. Cells have an area of 3 mm $\times$ 3 mm with a patterned area of 2 mm $\times$ 2 mm at the center. Cells were characterized in their initial state by external quantum efficiency (EQE) measurements on the 2 mm $\times$ 2 mm patterned area. The short circuit current density (J_{sc}) was calculated from each EQE curve, weighted by the AM1.5g spectrum and integrated over the wavelength range between 350 nm and 800 nm. Values of V_{oc} and FF are given in [26].

2.2. Optical simulations

The investigated structures were simulated optically with HFSS (High Frequency Structure Simulator), a software package based on the finite element method [29]. We used periodic boundary conditions along the x- and y-directions as illustrated in Fig. 1. In the out-of-plane direction, scattering boundary conditions were used. A three-dimensional mesh with adaptive spatial resolution was applied to calculate with high accuracy the electromagnetic field and corresponding parameters like light absorption in the regions of interest. Experimental ellipsometry data were used for the permittivities of the ZnO, silicon and ITO [47] films; different data sets for silver were taken from the literature as discussed above. The absorption in the intrinsic layer was used as a valid approximation for the external quantum efficiency of the solar cell. This simulation procedure has been successfully applied to simulate thin-film solar cells in a previous work [30]. Figure 1 shows that the silver nanoparticles are modelled as circular discs with a height of 40 nm and a diameter of 220 nm in a triangular grid where the center-to-center distance between adjacent particles is 430 nm. The ZnO layer is split into two 35-nm-thick layers for the nanoparticles reflector while it is taken as a single film of 70 nm for the grating reflector. The n- and p-doped layers are modelled as 15-nm-thick layers. As shown in our previous paper [26], the morphology near the front interface is changed due to non-conformal growth. Accordingly, Fig. 1 shows that the p-layer and the ITO film were modelled with a periodic pattern of hemispheric caps to resemble the front texture.

#190715 - $15.00 USD Received 17 May 2013; revised 4 Jul 2013; accepted 4 Jul 2013; published 16 Jul 2013

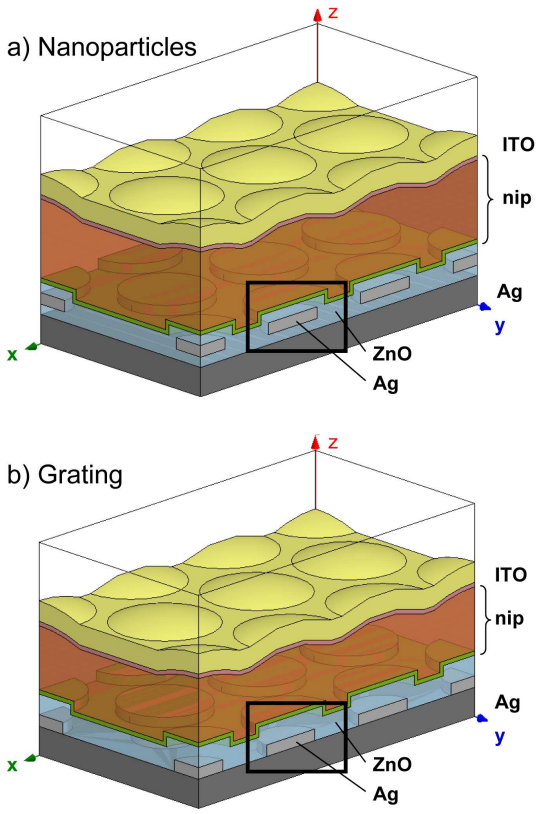

Fig. 1. Modelling domain used for the HFSS optical simulation. (a) Nanoparticles reflector with nanoparticles embedded in ZnO. (b) Grating reflector with nanoparticles in contact with the silver (Ag) layer. The silver nanoparticles are modelled as circular discs (light grey). The reminder of the cell-stack is identical in both configurations.

3. Results

3.1. Comparison of simulations with experimental EQEs

Measured and simulated external quantum efficiencies (EQEs) for the two configurations are shown in Fig. 2. Overall, it appears that the correspondence is better for the grating reflector while the modelling results overestimate the performance of the plasmonic grating. For wavelengths below 500 nm, this is most probably related to slight variations in the p-layer, which result in absorption losses of UV light, and to the ITO thickness, which shifts the position of the EQE maximum via its anti-reflection effect that is designed for 550 nm. The simulation input was not adapted since these films are at the very front and are thus minimally related to the back reflector strategy, the main topic of this contribution.

For wavelengths above 500 nm, in both panels, there is a multitude of peaks that are not apparent in the experimental EQEs since the grating periodicity as well as the shape of the nanoparticles is not perfect (see Fig. 2 in [26]). This point is discussed in Sect. 3.3. Nevertheless, if the experimental EQE enhancement with respect to the flat references is plotted, three clear resonances can be distinguished between 580 and 700 nm, and a fourth one at 750 nm is less pronounced [26]. We relate these signatures to guided modes whose excitation is mediated by grating coupling [31–34]. Since the grating period and the thickness of the guiding medium, i.e.

#190715 - $15.00 USD Received 17 May 2013; revised 4 Jul 2013; accepted 4 Jul 2013; published 16 Jul 2013

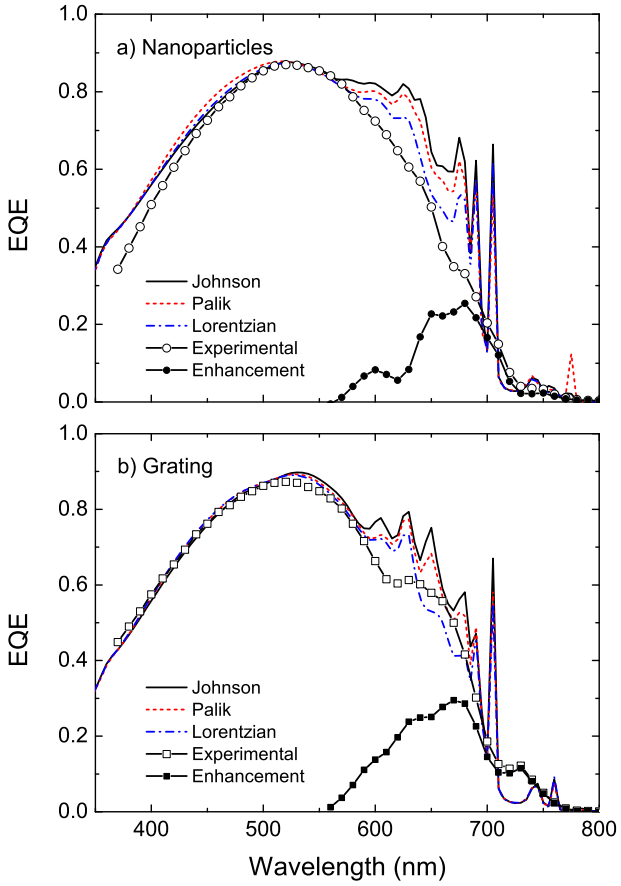

Fig. 2. Simulated and experimental EQEs of n-i-p a-Si:H solar cells deposited on the nanoparticles (a) and on the grating (b) reflectors, assuming different silver datasets. Large and small symbols represent the experimental EQEs and the enhancements with respect to a flat reference, respectively.

the silicon film, are identical, we can expect the guided modes to occur at the same wavelengths. However, they do differ in their respective intensities as the two types of back reflector have different coupling strengths. Sharpness of the resonances at long wavelengths can be related to the small absorption coefficient of silicon and the finite thickness of the cells [35, 36].

Experimentally, we do not have direct access to the dielectric properties of the silver used for the nanoparticles. Instead, we used tabulated data from the literature. The data of Johnson and Christie (in the subsequent text denoted simply by Johnson) [37] are widely used, as are those of Palik [38], which are very similar to the earlier data of Ingersoll [39]. Recently, it was suggested that neither Johnson nor Palik's data are representative [40] and that the data of Nash and Sambles [41] should be used instead. The comparison in Fig. 3 shows that the real parts of the various permittivities differ by about 10% or less in the wavelength range relevant for the current study. However, the logarithmic scale used for the imaginary part illustrates differences of almost one order of magnitude.

#190715 - $15.00 USD Received 17 May 2013; revised 4 Jul 2013; accepted 4 Jul 2013; published 16 Jul 2013

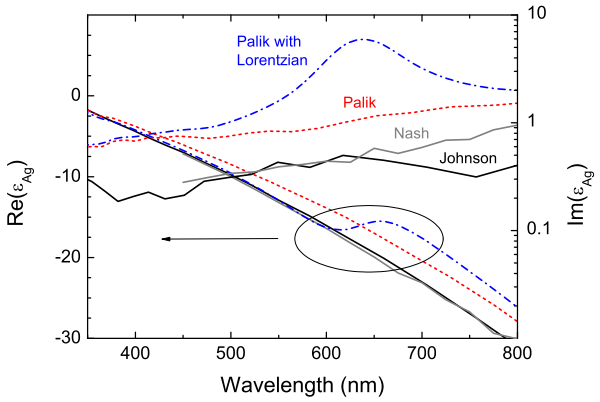

Fig. 3. Real and imaginary parts of the permittivity tabulated for silver. The uppermost curve corresponds to the data of Palik with the addition of a Lorentzian resonance at 1.95 eV. Note the logarithmic scale to the right for the imaginary part.

We chose the data with the largest and smallest imaginary part of silver permittivity – those of Palik and Johnson, respectively – over the light-trapping region, i.e. between 600 and 750 nm. The corresponding simulations result in the top two curves in Fig. 2. As expected from the low imaginary part, the data of Johnson predict the lowest losses in silver and therefore the highest EQEs between 600 and 700 nm. The response in this wavelength range is lower if data of Palik is used. For the grating reflector, the simulations start resembling the measured data with the exception of a small band between 600 and 650 nm where the EQE is still overestimated. For the nanoparticles reflector, however, both simulations are still significantly above the experimental characteristic.

3.2. Modification of material properties

From the previous section, it can be concluded that the material quality of silver is a decisive ingredient to high EQE in the light-trapping region. In other words, control of parasitic absorption in the metallic components is of key importance. Coming back to our experimental results, we can attempt to explain the remaining discrepancies by considering a silver layer that is even lossier than measured by Palik. Indeed, porosity and surface roughness have been reported to substantially increase parasitic losses in silver [42,43]. Based on a study of rough interfaces between silver and ZnO by real-time spectroscopic ellipsometry, Sainju et al. were able to extract the permittivity of an interfacial layer that represents intermixing of silver and ZnO [43]. The resulting characteristic resembles that of bulk silver, but with an added Lorentzian resonance whose amplitude and width are related to the effective thickness of the roughness zone. Following their approach, we define the permittivity of an interfacial layer by adding the susceptibility of a Lorentzian resonance to the dielectric data of Palik:

$$\chi(\omega) = A\frac{\Omega^2}{\Omega^2 - \omega^2 - i\Gamma\omega} \tag{1}$$

We used $\omega_1 = c/\lambda_1$, $\omega_2 = c/\lambda_2$, $\Omega = (\omega_1 + \omega_2)/2$, and $\Gamma = \omega_1 - \omega_2$ where c is speed of light in air. An amplitude of $A = 0.7$ and a wavelength window between $\lambda_1 = 600$ nm and $\lambda_2 = 675$ nm were chosen. The resulting permittivity is shown by the uppermost curve in Fig. 3. The addition of a Lorentzian resonance has a strong impact on the imaginary part of the permittivity over the resonant region while the changes to the real part are moderate.

#190715 - $15.00 USD Received 17 May 2013; revised 4 Jul 2013; accepted 4 Jul 2013; published 16 Jul 2013

For the sake of simplifying the modelling routine, we applied the modified permittivity to the whole volume of the silver nanoparticles. This might be justified to some extent for the nanoparticles reflector since in this case the particles are fully surrounded by ZnO and [43] reports that interfacial layers can be as thick as 25 nm. The choice is less justified for the grating reflector where only the side-walls and the upper surface are exposed to ZnO. The resulting simulations are represented by the lowest of the three lines in Fig. 2. This modification tends to underestimate the EQE on the grating reflector above 650 nm, but in the case of the plasmonic grating the simulated EQE is still above the experimental result. Hence, the parasitic loss is still not sufficient to account for the measurement on the nanoparticles grating. Despite all the weaknesses of this empirical approach, we can nevertheless infer that the nanoparticles reflector is more vulnerable to the parasitic absorption than the grating reflector since almost twice the surface area is exposed for intermixing with the surrounding ZnO.

3.3. Influence of particle geometry

The nanoparticle geometry has a significant influence on the resonance frequency and the associated light scattering [44]. To better reflect the SEM cross section images (see Fig. 3 in [26]), we replaced the discs with cropped cones with a wall inclination of 64.4° with respect to the substrate plane. The modelling results in Fig. 4 illustrate that this modification increases the EQE between 550 and 600 nm. It is unlikely that the marginally increased volume of the silicon absorber layer should yield such an improvement. Plotting the integrated absorption in the nanoparticles only, it appears that the gain in this spectral region is explained by reduced parasitic absorption. Figure 4 shows that on both types of reflector, the resonance at 710 nm is almost unchanged by the modification of the wall inclination. The peak at 680 nm undergoes a red-shift and a an intensity increase that is more pronounced on the grating reflector.

Figure 5 illustrates the changes that occur as the particles change from circular to oval discs that retain perpendicular side-walls. On the nanoparticles reflector, the resonance at 710 nm undergoes a noticeable blue-shift and a decrease in amplitude while the resonance at 680 nm is no longer distinguishable over the background of the steeply increasing EQE. The blue-shift is also observed on the grating reflector, but the decrease in intensity is much less pronounced. From this observation we conclude that the features around 700 nm are related to resonances of the nanoparticles. It appears that they respond to even the smallest deviation from a circular shape. In contrast to these sharp resonances, the broader ones at 600 and 620 nm are virtually unchanged, confirming the earlier association with modes in the silicon film. In order to account for experimental fluctuations, the solid line shows the average of the tree curves. Figure 5 shows a very good correspondence between simulations and experimental data in the resonant region around 700 nm.

4. Discussion

The results allow us to draw several conclusions about the functioning of plasmonic light scattering in solar cells. Figures 2, 4 and 5 show that in all modelled cases the nanoparticles reflector is predicted to achieve a higher EQE than the grating one. In terms of photocurrent, Table 1 shows that the difference amounts to 0.3 mA/cm^2, which is significant considering that the only difference between the reflectors is the position of the particles in the ZnO film. Yet higher gain may be expected simply by moving the particles closer to the absorber film [24].

We should still note that the idealized situation in the model does not reflect all experimental complications. In the following, we will discuss their impact on the shown results as well as possible remedies. First, it turned out that the dielectric data for silver given by Johnson are not necessarily representative of the experimental reality while the data tabulated by Palik appear to be better suited. The calculated integrated photocurrent is thus reduced by approximately

#190715 - $15.00 USD Received 17 May 2013; revised 4 Jul 2013; accepted 4 Jul 2013; published 16 Jul 2013

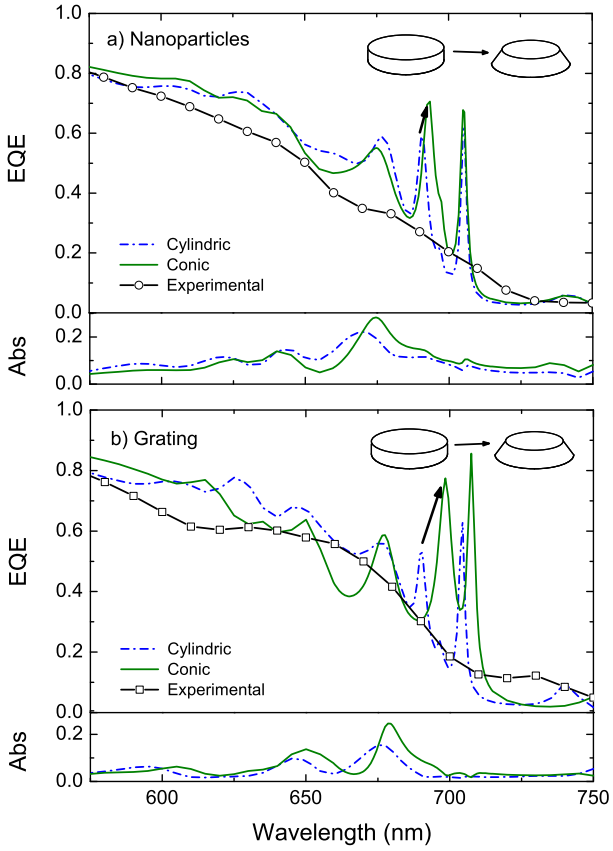

Fig. 4. Simulated and experimental EQEs for the nanoparticles (a) and the grating (b) reflectors, assuming cylindric (dashed-dotted lines) and conic (full lines) nanoparticles. In both panels, the lower part shows the absorption in the particles.

0.3 mA/cm^2 for both types of reflector. Compared to the material used in this investigation, higher quality silver can be obtained by depositing at elevated temperature or by annealing after deposition [45]; however, these two options can also change the morphology which would have been undesirable for the intended comparison. Finally, suppressing the sharp resonances around 700 nm yields a reduction of about 0.4 mA/cm^2. Again the value is almost exactly the same for the two types of reflector.

Another **experimental constraint** is surface roughness. This is hard to avoid in the real world and even more difficult to account for in simulation work. In the model, we kept Palik's data for the underlying silver layer but described the whole volume of nanoparticles as intermixed material. This yields a decrease of 0.5 mA/cm^2. Once more it is the same amount for both types of reflector.

Since the nanoparticles reflector is highly sensitive to the surface roughness and porosity of the nanoparticles, it will be mandatory to grow them under more suitable conditions and to improve the silver material quality. Sainju et al. recommended using polished wafer substrates

#190715 - $15.00 USD Received 17 May 2013; revised 4 Jul 2013; accepted 4 Jul 2013; published 16 Jul 2013

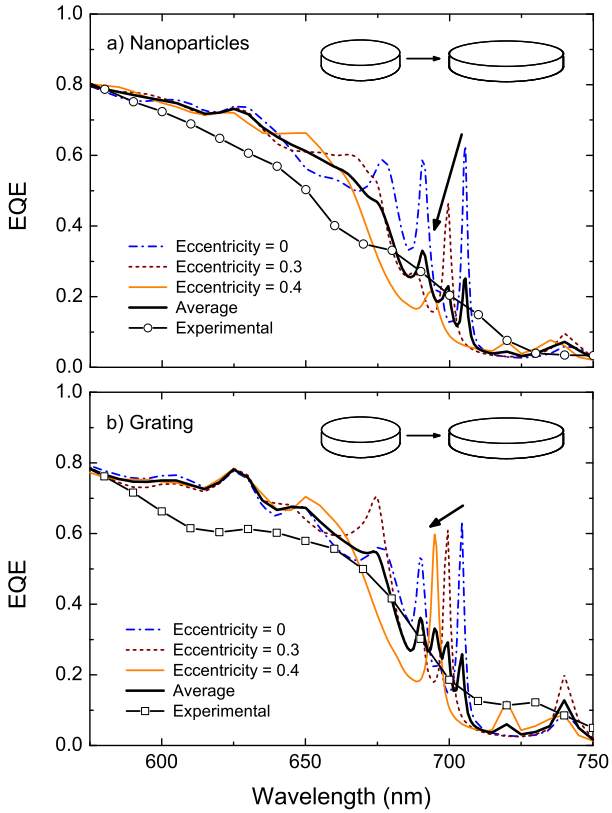

Fig. 5. Change of the EQE due to deviation of nanoparticle shape from circular to oval in the simulation. Dashed-dotted, dashed and full lines represent eccentricities of 0, 0.3 and 0.4, and the thick line gives their average. Circles and squares denote again the nanoparticles and the grating reflector, respectively.

and moderate power on the sputtering target in order to grow ultra-flat silver films [43]. In this experiment, the nanoparticles were fabricated by evaporation through a stencil membrane. However, thermal evaporation is known to provide growing films with very little energy for surface diffusion, often resulting in a porous microstructure [46]. We chose the evaporation process because its directionality was required for stencil lithography; without this constraint, better quality material can be obtained by choosing a different deposition process.

So far, all of the discussed losses were equally pronounced on the two reflector types. However, the design of this experiment unavoidably penalizes the nanoparticles concept: Even though care was taken to make the comparison as fair as possible, Fig. 6(b) shows that the particles in the grating reflector continue the grain structure of the flat silver film underneath. In case of the nanoparticles reflector shown in Fig. 6(a), the particles are forced to nucleate on the ZnO film, which is likely to result in a porous interface and a nucleation region with small grain size. Given the small height of the discs, the nucleation region will probably extend

#190715 - $15.00 USD Received 17 May 2013; revised 4 Jul 2013; accepted 4 Jul 2013; published 16 Jul 2013

Table 1. Short-circuit current densities for n-i-p cells on the nanoparticles and grating reflectors, using different dielectric data for the silver nanoparticles. Values in parentheses are obtained by suppressing the sharp resonances around 700 nm. The last line gives the experimental results [26].

Ag dataset	J_{sc} nanoparticles [mA/cm^2]	J_{sc} grating [mA/cm^2]
Jonhnson	15.39 (14.96)	15.14 (14.71)
Palik	15.16 (14.83)	14.88 (14.51)
Palik + Lorentzian res.	14.65 (14.25)	14.40 (14.00)
Experimental results	13.5	14.0

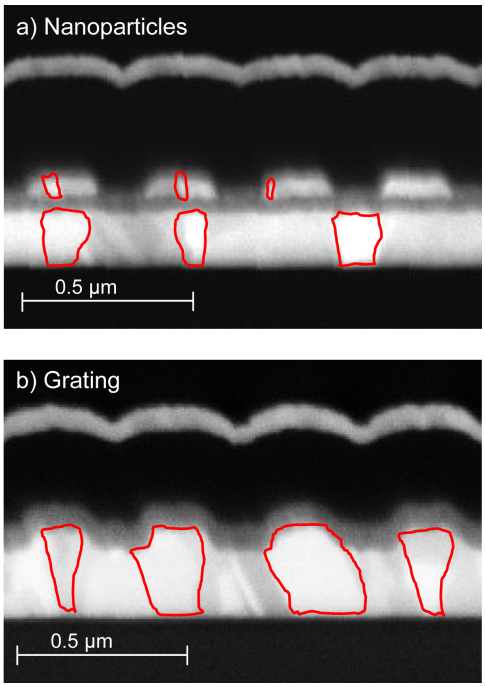

Fig. 6. SEM image cross section of a-Si:H solar cells deposited on the nanoparticles (a) and the grating reflectors (b). The silver nanoparticles in the nanoparticles reflector are composed of small silver grains due to their nucleation on the ZnO film while the silver grains can resume their growth in the grating reflector.

throughout most of each nanoparticle's volume. We chose the parameters of the Lorentzian resonance to show this effect, not to attain a perfect fit which would be physically meaningless with so crude a model. Our choice may therefore underestimate the losses in the nanoparticles case and overestimate those in the grating reflector where no intermixed zone is found at underside of the particles. Looking at the range of current densities with and without the presence of the Lorentzian resonance, we could argue that the grating reflector should be closer to 14.51 mA/cm^2 while the nanoparticles reflector might even dip below the projected value of 14.25 mA/cm^2.

#190715 - $15.00 USD Received 17 May 2013; revised 4 Jul 2013; accepted 4 Jul 2013; published 16 Jul 2013

5. Conclusion

We carried out a comparison between two strategies for the grating back reflector of thin-film solar cells. Using the same geometry, one is based on light scattering from localized plasmon resonances, and the other represents a conventional reflector with texture. Although the latter showed better light-trapping performance in our experiments and would discourage the use of nanoparticles concepts, theoretical modelling predicts otherwise. We studied a variety of scenarios to point out the adverse effects of the nanoparticles concept, in particular the poor quality of silver nanoparticles grown on the ZnO film. Finally we discussed alternative configurations and fabrication methods that could avoid these shortcomings and give plasmonic concepts a chance to live up to their potential and to exceed the photocurrent of state-of-the-art silicon solar cells.

Acknowledgement

The authors thank D. Alexander for the FIB and SEM images and V. Savu, M. Klein and J. Brugger for the deposition of silver nanodots. The authors acknowledge the support of the EU-Project Si-Light Contract No. 241277 and the Federal Office for Energy under Contract No. SI/500750-01.

#190715 - $15.00 USD Received 17 May 2013; revised 4 Jul 2013; accepted 4 Jul 2013; published 16 Jul 2013